CLEAN TECHNOLOGY, Vol. 20, No. 3, September 2014, pp. 306~313

청정에너지기술

Preparationand Characterization of Rutile-anatase Hybrid TiO_2 Thin Film by Hydrothermal Synthesis

Soon Jin Kwon[†], Hoon Sub Song[‡], Hyo Been Im[†], Jung Eun Nam[§]
Jin Kyu Kang[§], Taek Sung Hwang[#]*, and Kwang Bok Yi*

[†]Graduate School of Green Energy Technology, Chungnam National University
99 Daehak-ro, Yuseong-gu, Daejeon 305-764, Korea
[‡]Department of Chemical Engineering, University of Waterloo
200 University Avenue West, Waterloo, Ontario N2L3G1, Canada
[§]Advanced Convergence Research Center, Daegu Gyeongbuk Institute of Science & Technology
50-1, Sang-ri, Hyeonpung-myeon, Dalseong-gun, Daegu 711-873, Korea
[#]Department of Chemical Engineering, Chungnam National University
99 Daehak-ro, Yuseong-gu, Daejeon 305-764, Korea
Department of Chemical Engineering Education, Chungnam National University
99 Daehak-ro, Yuseong-gu, Daejeon 305-764, Korea

(Received for review June 18, 2014; Revision received July 17, 2014; Accepted July 17, 2014)

요 약

나노다공성 TiO_2 필름은 주로 염료감응형 태양전지의 작동전극으로 사용된다. 지금까지 염료감응형 태양전지의 광전환효율을 높이기 위해 TiO_2 나노구조체에 대한 다양한 연구가 시도되어왔다. 본 연구에서는 수열합성법을 이용하여 FTO glass 위에 루타일 TiO_2 나노로드를 수직적으로 성장시켰고 그 위에 아나타제 TiO_2 필름을 재 합성하였다. 이 새로운 방법은 아나타제 TiO_2 합성시 요구되는 시드층 합성단계를 피할 수 있었다. 밀집한 아나타제 TiO_2 층은 전자생성층으로써 고안되었고 시드층 대신 합성된 루타일 TiO_2 나노로드는 생성된 전자들이 FTO glass로 이동하는 통로역할을 하게 되었다. 전자이동률을 증진시키기 위해 루타일 나노로드에 $TiCl_4$ 수용액을 이용하여 표면 처리하였고 열처리 후 표면 위에 얇은 아나타제 TiO_2 필름을 형성시켰다. 합성된 루타일-아나타제 TiO_2 구조체의 두께는 4.5-5.0 μm이고 셀 테스트 결과 3.94%의 광전환효율을 얻게 되었다. 이는 루타일 TiO_2 나노로드 전극과 비교했을 때 광전환효율이 상당히 향상되는 것을 확인할 수 있었다.

주제어 : TiO_2 필름, 염료감응형 태양전지, 루타일-아나타제 TiO_2, 수열합성, $TiCl_4$ 처리

Abstract : Nanoporous TiO_2 films are commonly used as working electrodes in dye-sensitized solar cells (DSSCs). So far, there have been attempts to synthesize films with various TiO_2 nanostructures to increase the power-conversion efficiency. In this work, vertically aligned rutile TiO_2 nanorods were grown on fluorinated tin oxide (FTO) glass by hydrothermal synthesis, followed by deposition of an anatase TiO_2 film. This new method of anatase TiO_2 growth avoided the use of a seed layer that is usually required in hydrothermal synthesis of TiO_2 electrodes. The dense anatase TiO_2 layer was designed to behave as the electron-generating layer, while the less dense rutile nanorods acted as electron-transfer pathwaysto the FTO glass. In order to facilitate the electron transfer, the rutile phase nanorods were treated with a $TiCl_4$ solution so that the nanorods were coated with the anatase TiO_2 film after heat treatment. Compared to the electrode consisting of only rutile TiO_2, the power-conversion efficiency of the rutile-anatase hybrid TiO_2 electrode was found to be much higher. The total thickness of the rutile-anatase hybrid TiO_2 structures were around 4.5-5.0 μm, and the highest power efficiency of the cell assembled with the structured TiO_2 electrode was around 3.94%.

Keywords : TiO_2 film, Dye-sensitized solar cells (DSSCs), Rutile-anatase TiO_2, Hydrothermal synthesis, $TiCl_4$ treatment

1. Introduction

The recent acceleration in the pace of global warming has forced many researchers to focus on the development of alternative energy technologies such as solar cells and wind turbines that can replace a substantial portion of fossil fuels[1]. Among these alternatives, solar-cell technology is under active development owing to the possibility of instant application to the power

* To whom correspondence should be addressed.
E-mail: cosy32@cnu.ac.kr, tshwang@cnu.ac.kr http://cleantech.or.kr/ct/

doi: 10.7464/ksct.2014.20.3.306 pISSN 1598-9721 eISSN 2288-0690

supply chain[2]. Among solar cells, dye-sensitized solar cells (DSSCs) are considered more economically viable and environmentally friendly compared to silicon-based solar cells[2-5]. Titanium dioxide (TiO_2) has been adopted as an electrode material in DSSCs because of its promising characteristics as an n-type semiconductor. It has chemical and physical stability as well as a wide band-gap (3.2 eV) under ultraviolet light[6-8]. TiO_2 has three types of crystallographic structures: anatase, rutile, and brookite[9,10]. Anatase is known, despite its metastable characteristics at ambient temperature, to possess the highest photocatalytic activity because of its large surface area compared to rutile and brookite[11-14]. In addition, the anatase structure has low crystal-lattice packing fraction so that it absorbs light better owing to the reduced refractive index[15]. When anatase TiO_2 is heated above 500 ℃, it is irreversibly converted to the stable rutile structure[16,17]. Besides the physical and chemical properties of TiO_2, the geometry of the nanostructured TiO_2 electrode is a critical factor of the performance of DSSCs because the contour surface of the TiO_2 structure serves as a network of electron pathways[18-20]. Recently, various types of nanostructured TiO_2 such as nanoparticles, nanotubes, nanowires, and nanorods have been prepared and adopted as electrode materials to improve the performances of DSSCs[21-25]. Tan et al.[26] synthesized TiO_2 nanoparticles attached to TiO_2 nanowires to increase the surface area and applied them as a DSSC electrode material. They reported that the resulting DSSC had a power-conversion efficiency of 8.6%, which is 2% higher than the efficiency of the cell with a TiO_2 nanoparticle electrode. Lei et al.[27] grew TiO_2 nanotubes on Ti foil using the anodic oxidation method and prepared a cell that had a power-conversion efficiency of 8.07%. Therefore, it is believed that in addition to the requirement of a large surface area for dye absorption, a one-dimensional geometry of TiO_2 that provides straight pathways for electron transfer is essential to improve the solar-cell performance. If TiO_2 nanotubes are directly synthesized on fluorinated tin oxide (FTO) glass, which is not a commercially available technology at the current moment, higher cell performance might be achieved. Instead, researchers have focused on the direct growth on FTO glass of nanorods that possess characteristics similar to those of nanotubes[28-31]. In particular, rutile TiO_2 has a very small lattice mismatch (<2%) with FTO, and it is rather easy to grow rutile TiO_2 on FTO with large aspect ratios [32-34]. So far, it has been reported that rutile TiO_2 nanorods can be grown on FTO glass via hydrothermal synthesis[27-30]. For instance, Liu et al.[35] obtaineda DSSC power-conversion efficiency of 3% using TiO_2 nanorods that were grown to a length of up to 4 μm. In an advanced method, Wang et al.[36] attached TiO_2 nanobranches to the nanorods to increase the surface area and achieved a DSSC power-conversion efficiency of 3.75% even with nanorods that had heights of 3 μm. Nevertheless, it has been known that these forms of rutile TiO_2 are inferior to anatase TiO_2 in terms of DSSC power-conversion efficiency, and it is very difficult to grow anatase TiO_2 nanorods vertically on FTO glass because of the large lattice mismatch (~19%) between anatase TiO_2 and FTO[37,38]. Therefore, a TiO_2 colloid solution must be spin-coated onto the FTO glass in order to synthesize the layer of nanostructured anatase- phase TiO_2[39].

In this study, instead of using the thin TiO_2 seed layer, rutile TiO_2 nanorods were synthesized on FTO glass, on which the dense anatase TiO_2 nanostructures were fabricated using two different hydrothermal synthesis techniques in sequence. It was assumed that the electrons that were formed in the transparent anatase TiO_2 layerwould be transferred to the FTO glass through the rutile TiO_2 nanorods. In addition, the surfacesof the rutile TiO_2 nanorods were treated with aqueous $TiCl_4$ solutions that had varying concentrations of $TiCl_4$ for different treatment durations to prevent electron recombination[40].

2. Experimental

2.1. Preparation of TiO_2 nanostructures

Rutile-anatase hybrid TiO_2 nanostructures were prepared on FTO glass (TEC-8, 8 Ω/square) in two sequential hydrothermal-synthesis steps. The typical procedure is as follows: FTO glass was cleaned in a mixed solution of water, acetone, and 2-propanol (volume ratio = 1:1:1) in a sonication device for 30 min. After drying in ambient condition, the FTO glass was placed in a Teflon-lined stainless-steel vessel (100 mL). It was leaned against the vessel wall, with the conductive side facing down in a mixed solution containing 30 mL of de-ionized water, 30 mL of hydrochloric acid (36.5-38.0%, Sigma-Aldrich), and 0.5 mL of titanium butoxide (97%, Sigma-Aldrich). The stainless-steel vessel was then sealed and placed in a convective oven at 150 ℃ for 20 h. Following the procedure described above, rutile TiO_2 nanorods were vertically synthesized on FTO glass. The resulting sample was then rinsed with de-ionized water and immersed in an aqueous solution of $TiCl_4$ (0.2-0.4 M) and kept for 1-12 h at ambient temperature.

For the second hydrothermal synthesis, the rutile-covered FTO glass was washed with de-ionized water and dried. Next, the glass was placed in a mixed solution containing 35 mL of H_2O, 5 mL of sulfuric acid (ACS reagent, 95.0-98.0%, Sigma-Aldrich), and 2 mL of titanium butoxide (97%, Sigma-Aldrich) in the Teflon-lined stainless-steel vessel. Again, the steel vessel was placed in the convective oven at 180 ℃ and kept for 12 h. The resulting sample was removed, washed with de-ionized water, and dried. The sample was then calcined at 400 ℃ for 2 h. Finally, the rutile-anatase hybrid TiO_2 nanostructures were fabricated as a form of the anatase TiO_2 layer covering the upper tips of the

rutile TiO_2 nanorods on FTO glass. Hereafter, each sample is referred to as [R][$TiCl_4$ concentration]-[$TiCl_4$ treatment time][A]. The first letter R stands for rutile TiO_2, and the final letter A represents anatase TiO_2. For instance, to prepare the sample R0.2-12A, rutile TiO_2 nanorods were grown on FTO glass and then subjected to $TiCl_4$ (0.2 M) treatment for 12 h, during which anatase TiO_2 was synthesized on the nanorods.

2.2. Characterization of TiO_2 nanostructures

The crystal structure of the anatase TiO_2 nanostructures was characterized by X-ray diffraction (XRD Rigaku, 40 kV, 100 mA). The morphology of the samples was examined with a field-emission scanning electron microscope (FE-SEM S-4700, Hitachi) and a transmission electron microscope (TEM JEM-2100F HR, JEOL Ltd.) with an accelerating voltage of 200 keV, point resolution of 0.23 nm, and STEM resolution of 0.2 nm.

2.3. Assembling of dye-sensitized solar cells and their performance evaluation

The rutile-anatase TiO_2 electrodes were immersed in an ethanol solution of a ruthenium-complex (N719, Solaronix) for 24 h to complete the dye absorption. The FTO glass with 0.7 mm holes was coated with a 7 mM chloroplatinic acid (H_2PtCl_6, Aldrich) solution to serve as the counter electrode. The dye-absorbed TiO_2 electrode and Pt counter electrode were clamped firmly together with 60 mm-thick surlyn. The electrolyte containing 0.03 M I_2, 0.05 M LiI, 1 M 1-methyl-3-propylimidazolium iodide, 0.1 M guanidine thiocyanate, and 0.5 M *tert*-butyl pyridine in acetonitrile-valeronitrile (85:15) was injected into the clamped electrodes. The *I-V* characteristics of the DSSCs were measured with a Keithley 2400 source meter using an AM 1.5 (100 mW/cm^2) solar simulator equipped with a 1 kW xenon arc lamp (Oriel, Newport).

3. Results and Discussions

3.1. XRD analysis of the TiO_2 nanostructures

XRD analysis was carried out to determine the crystal structures of the prepared samples. The XRD patterns of the samples are shown in Figure 1. SnO_2 peaks appeared in all the patterns because FTO glass was used as the substrate. A comparison of the XRD pattern of sample R (Figure 1(a)) with the standard data in JCPDS 88-1175 confirmed the existence of rutile TiO_2, as shown by the (110) peak at 2θ = 27° and the (110) peak at 2θ = 54°. The XRD patterns of R0.2-1A (Figure 1(b)) and R0.4-12A (Figure 1(c)) show additional peaks at 2θ = 25°, 39°, 48°, 54°, and 55°, which match the diffraction peaks corresponding to the (101), (112), (200), (105), and (211) planes, respectively, of anatase TiO_2 according to JCPDS 84-1286. Therefore, it is clear that we obtained samples containing both rutile and anatase TiO_2 on FTO glass. As reflected by the samples' names, sample R is the one without $TiCl_4$ treatment of rutile TiO_2, while the other samples were treated with $TiCl_4$ solution before anatase TiO_2 was synthesized on the rutile TiO_2. Close examination of the XRD patterns of R and other samples revealed that the characteristic peaks of SnO_2 shifted slightly to the right. The enlarged view of XRD patterns for SnO_2 (101) peaks is shown in Figure 2. The (101) peak intensities of the rutile-anatase TiO_2 samples were much weaker than that of the rutile-only sample because anatase TiO_2 covered the rutile TiO_2 layers, limiting the

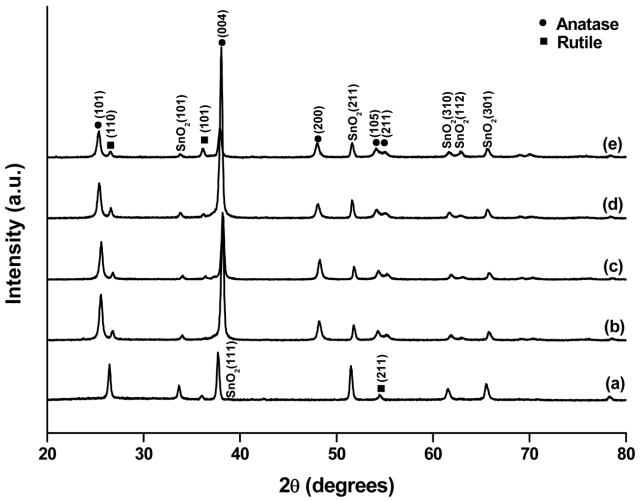

Figure 1. XRD patterns of TiO_2 nano-structures on FTO glass (a) R: rutile only, (b) R0.2-1A: rutile-anatase with $TiCl_4$ treatment (0.2 M, 1 h), (c) R0.2-12A: rutile-anatase with $TiCl_4$ treatment (0.2 M, 12 h), (d) R0.4-1A: rutile-anatase with $TiCl_4$ treatment (0.4 M, 1 h), (e) R0.4-12A: rutile-anatase with $TiCl_4$ treatment (0.4 M, 12 h).

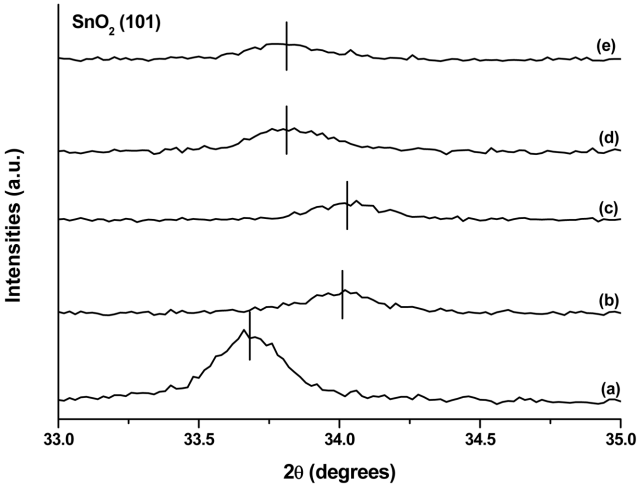

Figure 2. Enlarged XRD patterns showing shift of SnO_2 (101) peak according to the $TiCl_4$ treatment condition (a) R (b) R0.2-1A, (c) R0.2-12A, (d) R0.4-1A, (e) R0.4-12A.

depth of X-ray penetration. The extent of the peak shift depended on the concentration of $TiCl_4$ but not on the $TiCl_4$-treatment duration. When a lower concentration of $TiCl_4$ was applied, a longer exposure of the FTO glass surface to the $TiCl_4$ solution was expected because the amorphous TiO_2 deposition rate was slower than that with higher concentration of $TiCl_4$. Therefore, we believe that hydrogen chloride formed during the $TiCl_4$ treatment penetrated the rutile TiO_2 layer and attacked the exposed FTO surface, and some Sn atoms were replaced by Ti atoms that have a smaller atomic radius[41]. On the other hand, with a higher concentration of $TiCl_4$, the amorphous TiO_2 formation took place faster and covered the FTO surface quickly, preventing further attack of hydrogen chloride.

Another notable feature was that the characteristic peaks of the anatase TiO_2 in R0.4-1A and R0.4-12A (Figure 3(c), (d)) were located at positions that were slightly shifted to the left when compared to the same peaks of R0.2-1A and R0.2-12A (Figure 3(a), (b)). The peak shift implies that there was a change in the lattice parameters[42]. Table 1 shows the lattice parameters calculated from the (004) and (200) peaks of anatase TiO_2 in the samples. Even though the experimental conditions for the hydrothermal synthesis of anatase TiO_2 on the rutile TiO_2 layer were identical for all samples, the lattice parameters of each sample were varied. This phenomenon appears to be related to the concentration of the $TiCl_4$ solution, i.e., the lattice parameter *a* of the samples obtained with low $TiCl_4$ concentration appeared to be smaller than those of samples obtained with high $TiCl_4$ concentration, while the values of the lattice parameter *c* of all samples were similar.

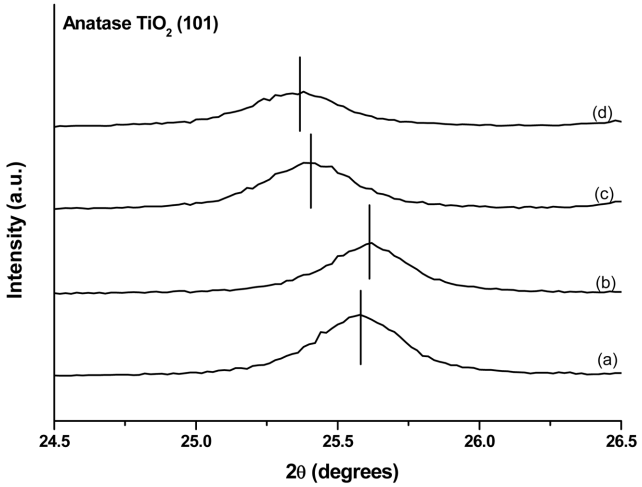

Figure 3. Enlarged XRD patterns showing shift of anatase TiO_2 (101) peak according to the $TiCl_4$ treatment (a) R0.2-1A, (b) R0.2-12A, (c) R0.4-1A, (d) R0.4-12A.

Table 1. Peak positions and lattice parameters of anatase TiO_2 in TiO_2 nano-structures

Sample names	Peak positions (2θ)		Lattice parameter (Å)	
	(004)	(200)	a	c
R0.2-1A	38.18	48.24	9.422	3.770
R0.2-12A	38.26	48.28	9.403	3.767
R0.4-1A	38.06	48.10	9.450	3.781
R0.4-12A	37.90	47.98	9.489	3.789

3.2. TEM and SEM analysis of the TiO_2 nanostructures

In order to investigate this variation in the lattice parameters of the anatase TiO_2 on rutile TiO_2, TEM analysis was carried out for rutile nanorods after $TiCl_4$ treatment. Figure 4 shows the TEM images of the rutile TiO_2 nanorods treated with $TiCl_4$at various concentrations and for different durations. When the concentration of $TiCl_4$ was 0.2 M, the amorphous TiO_2 layer was thin and uniform; and the thickness of the layer was affected by the treatment duration. On the other hand, when the concentration of $TiCl_4$ was 0.4 M, the amorphous TiO_2 layerwas much thicker than that obtained from the 0.2 M $TiCl_4$ solution, and an additional bulge corresponding to the rutile TiO_2 nanorods was observed. In addition, the thickness of the layer was proportional to the treatment time. Based on these observations,we believe that the less concentrated $TiCl_4$ solution provided the thin amorphous TiO_2 layer with the seeds for anatase TiO_2 growth. On the other hand, the high-concentration $TiCl_4$ solution provided more coarse and additional seeds apart from the surface of rutile TiO_2. Therefore, when a lower concentration of $TiCl_4$ was used, the resulting anatase TiO_2 tended to be packed and became denser towards the interior of the particles, creating a pressure that resulted in the smaller lattice parameter. Using a similar analysis approach, Zhang et al.[43] reported fabrication of CeO_2 and $BaTiO_3$ nanoparticle thin films in which the increased lattice parameter with decreasing particle size was explained by the negative effective pressure created by the competition between

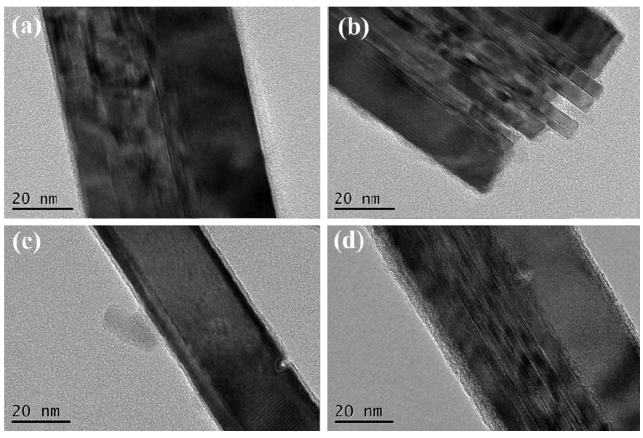

Figure 4. TEM images of rutile TiO_2 nanorods with $TiCl_4$ treatment; (a) 0.2 M-1 h, (b) 0.2 M-12 h, (c) 0.4 M-1 h, (d) 0.4 M-12 h.

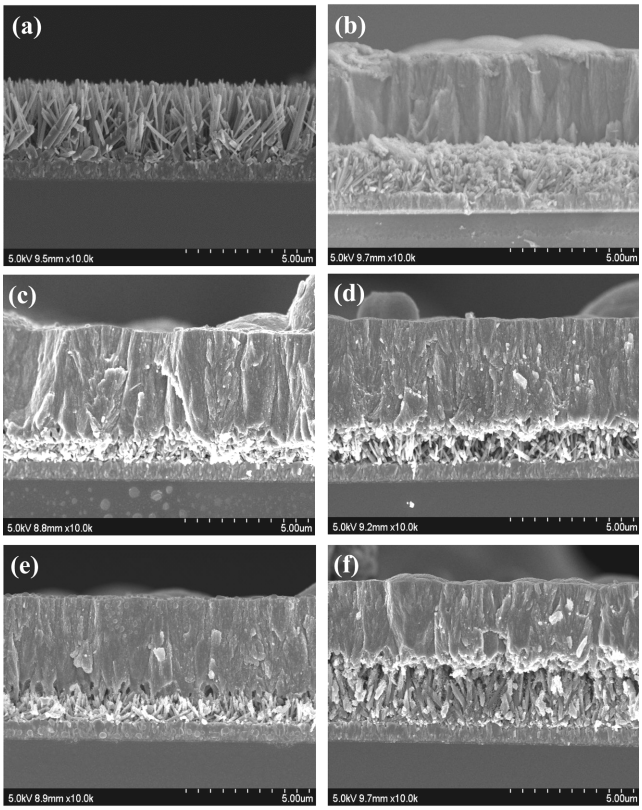

Figure 5. SEM images of TiO_2 nano-structures on FTO glass (a) R: rutile only, (b) RA: rutile-anatase without $TiCl_4$ treatment, (c) R0.2-1A: rutile-anatase with $TiCl_4$ treatment (0.2 M, 1 h), (d) R0.2-12A: rutile-anatase with $TiCl_4$ treatment (0.2 M, 12 h), (e) R0.4-1A: rutile-anatase with $TiCl_4$ treatment (0.4 M, 1 h), (f) R0.4-12A: rutile-anatase with $TiCl_4$ treatment (0.4 M, 12 h)

the long-range Coulomb attractive interactions and the short-range repulsive interactions in ionic nanocrystals. Li et al.[44] also reported that the concurrent packed growth of rutile TiO_2 physically squeezed the anatase TiO_2 phase, resulting in a decrease in the lattice parameter.

The SEM images in Figure 5 show that the rutile TiO_2 nanorods were well grown like mowed grass, as reported by Liu et al.[35]. The concentration of the precursor and other chemicals were adjusted by trial and error until the proper density of nanorods was obtained. In the image of sample RA (Figure 5(b)), whose anatase TiO_2 layer was deposited on the rutile TiO_2 nanorods without $TiCl_4$ treatment, it can be seen that the dense, powder-like anatase TiO_2 grew and filled all the gaps between the nanorods. On the other hand, when the rutile TiO_2 was treated with $TiCl_4$ prior to the anatase TiO_2 synthesis (Figure 5(c-f)), the anatase phase was confirmed to grow on the tips of the rutile nanorods, leaving the gaps between the nanorods empty[45]. It should be noted that these empty gaps played very important roles in the DSSC performance. When incident light came in through the anatase layer, this empty space allowed the light to reflect multiple times and remained for a longer period in the TiO_2 structure to produce more electrons. According to the SEM images, the height of the rutile nanorods was strongly dependent on both the concentration of $TiCl_4$ and $TiCl_4$ treatment duration. The rutile nanorod layer in R0.2-1A was barely recognizable, while the thicker layer of the nanorods in R0.2-12A was clearly distinguishable and showed more empty space. This means that the height of rutile nanorods increased with longer $TiCl_4$-treatment duration. This relationship was also observed in R0.4-1A and R0.4-12A. On the other hand, treatment at a higher concentration of $TiCl_4$ for the same amount of time contributed to the growth of the nanorod radius. It should be carefully considered that the rutile nanorods in sample R were shortened with $TiCl_4$ treatment it has been reported that the$TiCl_4$ solution has an etching effect on rutile nanorods[46,47]. It has also been reported that rutile nanorods grow with extended $TiCl_4$ treatment[47]. These reports match our experimental results that showed the height of the nanorods decreased in the following order: R0.4-12A > R0.2-12A > R0.4-1A > R0.2-1A.

3.3. Power-conversion efficiency

The power-conversion efficiency of a DSSC strongly depends on the geometric configuration and thickness of the TiO_2 structure. As shown in the SEM image analysis, the six TiO_2 structures on FTO glass showed clear differences in thickness and geometric configuration. The current density-voltage (*J-V*) responses for all solar cells assembled with the six samples are plotted in Figure 6. The photovoltaic characteristics of the DSSCs were summarized in Table 2. The fill factor (*FF*) and open circuit voltage (V_{OC}) showed small variations among DSSCs assembled with the samples. Even though the values of total

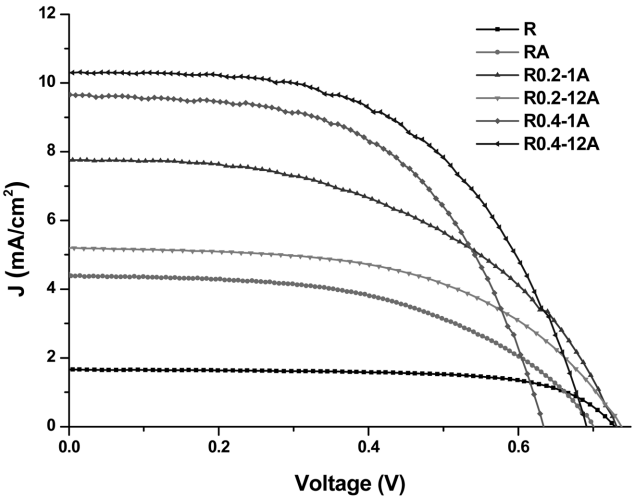

Figure 6. J -V curves of the DSSCs assembled with from TiO_2 nanostructures (a) R, (b) RA, (c) R0.2-1A, (d) R0.2-12A, (e) R0.4-1A, (f) R0.4-12A.

Table 2. Photovoltaic characteristics of DSSCs assembled with TiO_2 nano-structures

Sample	V_{oc} (V)	J_{sc} (mA/cm^2)	FF	η (%)
R	0.73	1.65	0.67	0.81
RA	0.70	4.38	0.51	1.59
R0.2-1A	0.73	7.76	0.50	2.83
R0.2-12A	0.74	5.19	0.54	2.08
R0.4-1A	0.63	9.74	0.56	3.45
R0.4-12A	0.69	10.30	0.55	3.94

thickness of the TiO_2 nanostructures (4.5-5.0 μm) were very similar, the photovoltaic characteristics were clearly different. As expected, the cell prepared from the sample with only rutile nanorods on FTO glass (sample R) showed the lowest short-circuit current density (J_{SC}) of 1.65 mA/cm^2 with doubled power-conversion efficiency (*PCE*) of 0.81%. When anatase was deposited on the rutile nanorods without $TiCl_4$ treatment (sample RA), J_{SC}increased to 4.38 mA/cm^2 with doubled *PCE*. The cell assembled with R0.2-1A showed significantly increased values of J_{SC} and *PCE* compared to 7.76 mA/cm^2 and 2.83%, respectively, for the cell assembled with RA. This implies the rutile structure under the anatase layer acted as an effective pathway for the electrons generated within the anatase layer. However, the cell with R0.4-12A that had a layer of longer rutile nanorods exhibited J_{SC} of 5.19 mA/cm^2 and *PCE* of 2.08%, which are lower than those of the cell assembled with R0.2-1A. Even with the longer rutile nanorod layer, the low density of the nanorods appeared to limit the rate of electron transfer. As further evidence, the cell with R0.4-1A that had nanorods with similar height but at higher density showed much higher J_{SC} of 9.74 mA/cm^2 and *PCE* of 3.45%. Finally, the cell with R0.4-12A exhibited the highest J_{SC} and *PCE* of 10.3 mA/cm^2 and 3.94%, respectively. Careful examination of the SEM image of R0.4-12A revealed that the nanorods were much thicker and taller than others with relatively high density. Therefore, it is reasonable to assume that the physical shape and size of the nanorods were the main factors that affected the performance of the DSSCs. The nanorods should have both high density and long length so that light can reflect back and forth under the anatase layer, producing electrons both inside the thick anatase layer and the anatase covering the rutile nanorods.

4. Conclusions

In this study, rutile-anatase hybrid TiO_2 nanostructures were prepared and characterized. DSSCs were assembled with the prepared TiO_2 nanostructures and their photovoltaic characterizations were obtained. The rutile nanorods were found to act as effective pathways for the electrons produced in the anatase layer. It was confirmed that the rutile nanorods should have high length and relatively high density to increase *PCE* of the DSSC. The empty space between the nanorods was a very important factor of *PCE* because it facilitated the light reflection within the nanorod layer to producing more electrons.

Acknowledgment

This work was supported by research fund of 2014 Chungnam National University.

References

1. Granovskii, M., Dincer, I., and Rosen, M. A., "Greenhouse Gas Emissions Reduction by Use of Wind and Solar Energies for Hydrogen and Electricity Production: Economic Factors," *Int. J. Hydro. Energ.*, **32**, 927-931 (2007).
2. Lee, H. J., Park, N. K., Lee, T. J., Han, G. B., and Kang, M. S., "Effect of Particle Size and Structure of TiO_2 Semiconductor on Photoelectronic Efficiency of Dye-sensitized Solar Cell," *Clean Technol.*, **19**, 22-29 (2013).
3. Regan, B. O., and Grätzel, M., "A Low-cost, High-efficiency Solar Cell Based on Dye-sensitized Colloidal TiO_2 Films," *Nature*, **353**, 737-740 (1991).
4. Grätzel, M., "Solar Energy Conversion by Dye-Sensitized Photovoltaic Cells," *Inorg. Chem.*, **44**, 6841-6851 (2005).
5. Grätzel, M., "Recent Advances in Sensitized Mesoscopic Solar Cells," *Acc. Chem. Res.*, **42**, 1788-1798 (2009).
6. Frank, S. N., and Bard, A. J., "Semiconductor Electrodes. II. Electrochemistry at n-Type TiO_2 Electrodes in Acetonitrile Solutions," *J. Am. Chem. Soc.*, **97**, 7427-7433 (1975).
7. Santz, P. A., and Kamat, P. V., "Interparticle Electron Transfer between Size-quantized CdS and TiO_2 Semiconductor Nanoclusters," *Phys. Chem. Chem. Phys.*, **4**, 198-203 (2002).
8. Giraudeau, A., Fan, F. F., and Bard, A. J., "Semiconductor Electrodes. 30. Spectral Sensitization of the Semiconductors n-$TiO_2$and n-WO_3 with Metal Phthalocyanines," *J. Am. Chem. Soc.*, **102**, 5142-5148 (1980).
9. Mo, S. D., and Ching, W. Y., "Electronic and Optical Properties of Three Phases of Titanium Dioxide: Rutile, Anatase, and Brookite," *Phys. Rev.,* **B51**, 13023-13032 (1995).
10. Reintjes, J., and Schultz, M. B., "Photoelastic Constants of Selected Ultrasonic Delay-Line Crystals," *J. Appl. Phys.*, **39**, 5254-5258 (1968).
11. Chen, D., Huang, F., Cheng, Y. B., and Caruso, R. A., "Mesoporous Anatase TiO_2 Beads with High Surface Areas and Controllable Pore Sizes: A Superior Candidate for High-Performance Dye-Sensitized Solar Cells," *Adv. Mater.*, **21**, 2206-2210 (2009).
12. Barbe, C. J., Arendse, F., Comte, P., Jirousek, M., Lenzmann, F., Shklover, V., and Grätzel, M., "Nanocrystalline Titanium Oxide Electrodes for Photovoltaic Applications," *J. Am. Ceram.*

Soc., **80**, 3157-3171 (1997).
13. Chou, T. P., Zhang, Q. F., Russo, B., Fryxell, G. E., and Cao, G. Z., "Titania Particle Size Effect on the Overall Performance of Dye-Sensitized Solar Cells," *J. Phys. Chem. C*, **111**, 6296-6302 (2007).
14. Cahen, D., Hodes, G., Grätzel, M., Guillemoles, J. F., and Riess, I., "Nature of Photovoltaic Action in Dye-Sensitized Solar Cells," *J. Phys. Chem. B*, **104**, 2053-2059 (2000).
15. Miao, L., Jin, P., Kaneko, K., Terai, A., Nabatova-Gabain, N., and Tanemura, S., "Preparation and Characterization of Polycrystalline Anatase and Rutile TiO_2 Thin fims by rf Magnetron Sputtering," *App. Surf. Sci.*, **212**, 255-263 (2003).
16. Zhang, Q., Gao, L., and Guo, J., "Effects of Calcination on the Photocatalytic Properties of Nanosized TiO_2 Powders Prepared by $TiCl_4$ Hydrolysis," *Appl. Catal. B-Environ.*, **26**, 207-215 (2000).
17. Ovenstone, J., and Yanagisawa, K., "Effect of Hydrothermal Treatment of Amorphous Titania on the Phase Change from Anatase to Rutile during Calcination," *Chem. Mater.*, **11**, 2770-2774 (1999).
18. Benkol, G., Kallioinen, J., Myllyperkio1, P., Trif, F., Tommola, J. E. I. K., Yartsev, A. P., and Sundstrom, V., "Interligand Electron Transfer Determines Triplet Excited State Electron Injection in RuN_3-Sensitized TiO_2 Films," *J. Phys. Chem. B*, **108**, 2862-2867 (2004).
19. Yu, H., Zhang, S., Zhao, H., Xue, B., Liu, P., and Will, G., "High-Performance TiO_2 Photoanode with an Efficient Electron Transport Network for Dye-Sensitized Solar Cells," *J. Phys. Chem. C*, **113**, 16277-16282 (2009).
20. Palomares, E., Clifford, J. N., Haque, S. A., Lutz, T., and Durrant, J. R., "Slow Charge Recombination in Dye-sensitised Solar Cells (DSSC) Using Al_2O_3 Coated Nanoporous TiO_2 Films," *Chem. Comm.*, 1464-1465 (2002).
21. Jennings, J. R., Ghicov, A., Peter, L. M., Schmuki, P., and Walker, A. B., "Dye-Sensitized Solar Cells Based on Oriented TiO_2 Nanotube Arrays: Transport, Trapping, and Transfer of Electrons," *J. Am. Chem. Soc.*, **130**, 13364-13372 (2008).
22. Liu, Z., Subramania, V. R., and Misra, M., "Vertically Oriented TiO_2 Nanotube Arrays Grown on Ti Meshes for Flexible Dye-Sensitized Solar Cells," *J. Phys. Chem. C*, **113**, 14028-14033 (2009).
23. Feng, X., Shankar, K., Paulose, M., and Grimes, C. A., "Tantalum-Doped Titanium Dioxide Nanowire Arrays for Dye-Sensitized Solar Cells with High Open-Circuit Voltage," *Angew. Chem.*, **121**, 8239-8242 (2009).
24. Albu, S. P., Kim, D., and Schmuki, P., "Growth of Aligned TiO_2 Bamboo-Type Nanotubes and Highly Ordered Nanolace," *Angew Chem.*, **120**, 1942-1945 (2008).
25. Kuang, D., Brillet, J., Chen, P., Takata, M., Uchida, S., Miura, H., Sumioka, K., Zakeeruddin, S. M., and Grätzel, M., "Application of Highly Ordered TiO_2 Nanotube Arrays in Flexible Dye-Sensitized Solar Cells," *ACS Nano.*, **2**, 1113-1116 (2008).
26. Tan, B., and Wu, Y., "Dye-Sensitized Solar Cells Based on Anatase TiO_2 Nanoparticle/Nanowire Composites," *J. Phys. Chem. B*, **110**, 15932-15938 (2006).
27. Lei, B. X., Liao, J. Y., Zhang, R., Wang, J., Su, C. Y., and Kuang, D. B., "Ordered Crystalline TiO_2 Nanotube Arrays on Transparent FTO Glass for Efficient Dye-Sensitized Solar Cells," *J. Phys. Chem. C*, **114**, 15228-15233 (2010).
28. Pommer, E. E., Liu, B., and Aydil, E. S., "Electron Transport and Recombination in Dye-sensitized Solar Cells Made from Single-crystal Rutile TiO_2 Nanowires," *Phys. Chem. Chem. Phys.*, **11**, 9648-9652 (2009).
29. Feng, X., Zhu, K., Frank, A. J., Grimes, C. A., and Mallouk, T. E., "Rapid Charge Transport in Dye-Sensitized Solar Cells Made from Vertically Aligned Single-Crystal Rutile TiO_2 Nanowires," *Angew. Chem.*, **124**, 2781-2784 (2012).
30. Huang, Q., Zhou, G., Fang, L., Hua, L., and Wang, Z. S., "TiO_2 Nanorod Arrays Grown from a Mixed Acid Medium for Efficient Dye-sensitized Solar Cells," *Energy Environ. Sci.*, **4**, 2145-2151 (2011).
31. Lv, M., Zheng, D., Ye, M., Sun, L., Xiao, J., Guo, W., and Lin, C., "Densely Aligned Rutile TiO_2 Nanorod Arrays with High Surface Area for Efficient Dye-sensitized Solar Cells," *Nanoscale*, **4**, 5872-5879 (2012).
32. Howard, C. J., Sabine, Z. M., and Dickson, F., "Structural and Thermal Parameters for Rutile and Anatase," *Acta Cryst. B*, **47**, 462-468 (1991).
33. Sedach, P. A., Gordon, T. J., Sayed, S. Y., Fürstenhaupt, T., Sui, R., Baumgartner, T., and Berlinguette, C. P., "Solution Growth of Anatase TiO_2 Nanowires from Transparent Conducting Glass Substrates," *J. Mater. Chem.*, **20**, 5063-5069 (2010).
34. Wang, X., Liu, Y., Zhou, X., Li, B., Wang, H., Zhao, W., Huang, H., Liang, C., Yu, X., Liua, Z., and Wang, H. S., "Synthesis of Long TiO_2 Nanowire Arrays with High Surface Areas via Synergistic Assembly Route for Highly Efficient Dye-sensitized Solar Cells," *J. Mater. Chem.*, **22**, 17531-17538 (2012).
35. Liu, B., and Aydil, E. S., "Growth of Oriented Single-Crystalline Rutile TiO_2 Nanorods on Transparent Conducting Substrates for Dye-Sensitized Solar Cells," *J. Am. Chem. Soc.*, **131**, 3985-3990 (2009).
36. Wang, H., Bai, Y., Wu, Q., Zhou, W., Zhang, H., Li, J., and Guo, L., "Rutile TiO_2 Nano-branched Arrays on FTO for Dye-sensitized Solar Cells," *Phys. Chem. Chem. Phys.*, **13**, 7008-7013 (2011).
37. Feng, X., Shankar, K., Paulose, M., and Grimes, C. A., "Tantalum-Doped Titanium Dioxide Nanowire Arrays for Dye-Sensitized Solar Cells with High Open-Circuit Voltage," *Angew. Chem. Int. Ed. Engl.*, **48**, 8095-8098 (2009).
38. Wu, W. Q., Lei, B. X., Rao, H. S., Xu, Y. F., Wang, Y. F., Su, C. Y., and Kuang, D. B., "Hydrothermal Fabrication of Hierarchically Anatase TiO_2 Nanowire Arrays on FTO Glass for Dye-sensitized Solar Cells," *Sci Rep.*, **3**, 1352 (2013).

39. Liao, J. Y., Lei, B. X., Wang, Y. F., Liu, J. M., Su, C. Y., and Kuang, D. B., "Hydrothermal Fabrication of Quasi-One-Dimensional Single-Crystalline Anatase TiO_2 Nanostructures on FTO Glass and Their Applications in Dye-Sensitized Solar Cells," *Chem. Eur. J.*, **17**, 1352-1357 (2011).
40. Charoensirithavorn, P., Ogomi, Y., Sagawa, T., Hayase, S., and Yoshikawa, S., "Improvement of Dye-Sensitized Solar Cell Through $TiCl_4$-Treated TiO_2 Nanotube Arrays," *J. Electrochem. Soc.*, **157**, B354-B356 (2010).
41. Teatum, E. T., Gschneidner, K. A., and Waber, J. T., "Compilation of Calculated Date Useful in Predicting Metallurgical Behavior of the Elements in Binary Alloy System," *Nat. Technol. Inf. Ser.*, **206**, (1968).
42. Ungar, T., "Microstructural Parameters from X-ray Diffraction Peak Broadening," *Scr. Mater.*, **51**, 777-781 (2004).
43. Zhang, F., Chan, S. W., Spanier, J. E., Apak, E., Jin, Q., Robinson, R. D., and Herman, I. P., "Cerium Oxide Nanoparticles: Size-selective Formation and Structure Analysis," *Appl. Phys. Lett.*, **80**, 127-129 (2002).
44. Li, W., Ni, C., Lin, H., Huang, C. P., and Shah, S. I., "Size Dependence of Thermal Stability of TiO_2 Nanoparticles," *J. Appl. Phys.*, **96**, 6663-6668 (2004).
45. Cho, T. Y., Han, C. W., Jun, Y. S., and Yoon, S. G., "Formation of Artificial Pores in Nano-TiO_2 Photo-electrode Films Using Acetylene-black for High-efficiency, Dye-sensitized Solar Cells," *Sci. Rep.*, **3**, 1496 (2013).
46. Kim, S. Y., and van Duin, A. C. T., "Simulation of Titanium Metal/Titanium Dioxide Etching with Chlorine and Hydrogen Chloride Gases Using the ReaxFF Reactive Force Field," *J. Phys. Chem. A*, **117**, 5655-5663 (2013).
47. Guo, W., Xu, C., Wang, X., Wang, S., Pan, C., Lin, C., and Wang, Z. L., "Rectangular Bunched Rutile TiO_2 Nanorod Arrays Grown on Carbon Fiber for Dye-Sensitized Solar Cells," *J. Am. Chem. Soc.*, **134**, 4437-4441 (2012).